ACS OMEGA

Article

Cite This: ACS Omega 2019, 4, 16292−16299

http://pubs.acs.org/journal/acsodf

Rapid Prototyping of an Open-Surface Microfluidic Platform Using Wettability-Patterned Surfaces Prepared by an Atmospheric-Pressure Plasma Jet

She-Ting Wu,[†] Chen-Yu Huang,[‖] Chih-Chiang Weng,[⊥] Chia-Chih Chang,[†] Bor-Ran Li,[*,‡,§] and Chain-Shu Hsu[*,†,§]

[†]Department of Applied Chemistry, [‡]Institute of Biomedical Engineering, and [§]Center for Emergent Functional Matter Science, National Chiao Tung University, 1001 Ta Hsueh Road, Hsinchu 30049, Taiwan

[‖]Department of Physics and Astronomy, Johns Hopkins University, 3400 N. Charles St., Baltimore, Maryland 21218, United States

[⊥]Mechanical and Mechatronics Systems Research Laboratories, Industrial Technology Research Institute, Hsinchu 31040, Taiwan

Supporting Information

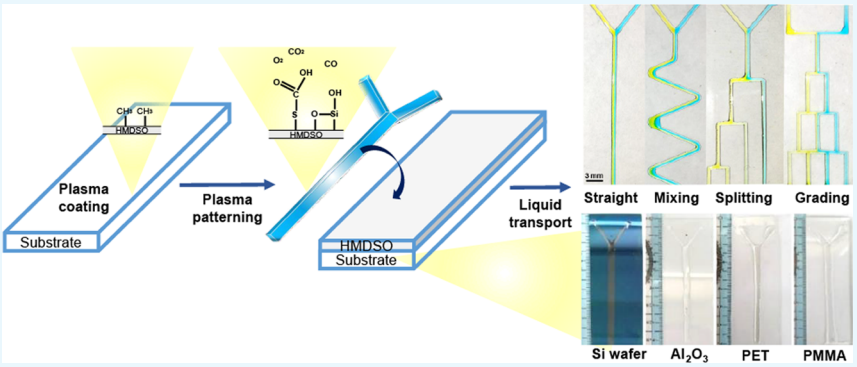

ABSTRACT: Open-surface microfluidics is promising in terms of enabling economical and rapid biochemical analysis for addressing challenges associated with medical diagnosis and food safety. To this end, we present a simple and economical approach to develop an open-surface microfluidic platform suitable for facile liquid transport and mixing. Customizable patterns with tailored wettability are deposited using a plasma-assisted deposition technique under atmospheric pressure. The flow of the dispensed liquid is driven by gravity, and the tilting angle of the device determines the extent of mixing. First, a hexamethyldisiloxane film was deposited to create hydrophobic patterns on glass, and then, hydrophilic acrylic acid was deposited by a patterned cardboard mask to construct a channel suitable for forming channels to transport aqueous liquids without the need of an external energy input; the liquid can be confined to designated pathways. Several designs including Y-junctions, serpentine-shaped patterns, splitting channels, and concentration gradient generation patterns are presented. The proposed method can spatially pattern a surface with a hydrophobic/hydrophilic area, which can function as a microfluidic channel, and the surface can be applied in microfluidic devices with other types of substrates.

INTRODUCTION

In recent years, biosensors have drawn considerable research attention because of their potential to rapidly diagnose several diseases. Notable biosensor types include a surface plasmon resonance biosensor,[1] a silicon nanowire field-effect transistor,[2] and a quartz crystal microbalance.[3] The underlying working mechanisms of various biosensors, including their simplicity and ease of implementation, are crucial in the design of sensing devices. Furthermore, clinical specimens must be transported to the sensing area of the device through a reliable microfluidic system.[4−6]

Among these diagnostic platforms, open-surface microfluidic systems have become increasingly popular because of their potential for use in point-of-care diagnostics and lab-on-chip applications.[7−9] Compared with other microfluidic systems, open-surface microfluidics have emerged as a user friendly approach to construct multifunctional devices.[10−13] For instance, open-surface microfluidics can be integrated with other advanced analytical techniques such as electrochemical sensing and fluorescence detection.[10] The simplicity of the fabrication technique bears critical importance with respect to the development of open-surface microfluidic technologies.[11] In such open-surface microfluidic systems, gravity-driven fluid transport that does not require any external energy input is of particular interest. Typically, a wettability contrast can be created by depositing a hydrophilic pattern onto a hydro-

Received: May 7, 2019
Accepted: September 18, 2019
Published: September 26, 2019

DOI: 10.1021/acsomega.9b01317
ACS Omega 2019, 4, 16292−16299

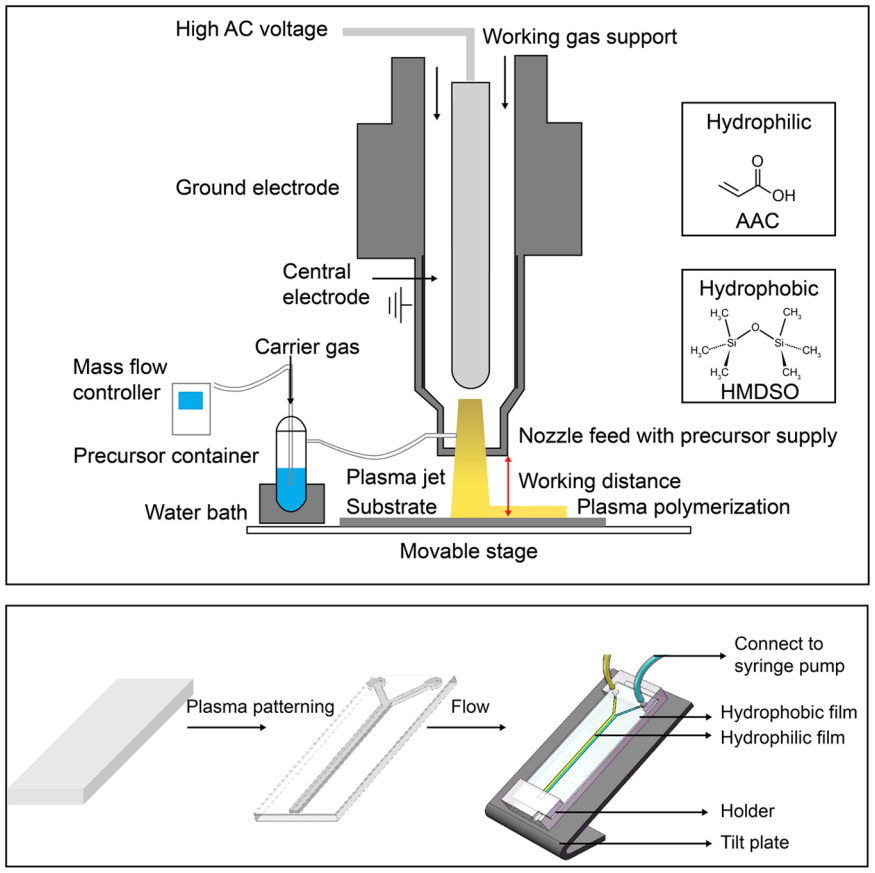

Figure 1. Schematic of the atmospheric-pressure plasma jet (APPJ) setup and open-surface microfluidic platform setup; the two types of wettability precursors used to form open-surface microfluidic by plasma patterning: AAC-modified (top layer) and HMDSO-modified (bottom layer) on glass.

phobic substrate, thereby enabling localized entrapment.[12,13] As such, the liquid flows to the designated hydrophilic area owing to surface tension.[14] The liquid movement can be manipulated by synchronizing the effects of surface energy, liquid surface tension, and device geometry.[15] For example, Melin et al. proposed the application of an open microchannel system in a pressure-driven continuous flow.[16] The proposed device structure comprised a glass substrate with a 100 μm-thick polydimethylsiloxane (PDMS) film. The open part of the channel was cut into the PDMS layer. This open structure of the demonstrated system leverages the benefits of accessibility and reliability when employed in microfluidic systems. Berthier et al.[17] reported the use of a capillary-driven microfluidic system, wherein a spontaneous capillary flow can be established within the suspended channel of an open-surface substrate. A long, suspended channel was fabricated by milling through a 1 mm-thick PMMA plate, where liquid flow was suspended between two parallel vertical walls.

Thus far, hydrophilic tracks have been created using surface-modification techniques, such as UV irradiation,[15] photochemical grafting,[18] and chemical vapor deposition[19] under vacuum conditions to modify surface properties. The use of an atmospheric-pressure plasma jet (APPJ) allows for the deposition of heavily cross-linked films on various surfaces sans the need for a high-vacuum environment and associated pumping (chamber system). The APPJ treatment[20] is a dry process that generates plasma under atmospheric conditions, thereby saving money and time. In addition to these advantages, the process is rapid and environmentally friendly.[21] The APPJ treatment is suitable for integration in inline processes and can also be used for surface property control applications, such as surface activation and coating.[21−24] The APPJ facilitates the facile creation of hydrophilic channels by employing a simple cardboard-based mask.[25−27]

Plasma-polymerized hexamethyldisiloxane (HMDSO) is a widely used material because of its characteristics, such as good adherence to glass, high chemical stability, transparency, and scratch resistance. More importantly, HMDSO deposition on glass renders modified surfaces hydrophobic, as evidenced by a water contact angle exceeding 90°. Hydrophobic surfaces are generally used considering their ability to repel biological specimens. Therefore, plasma-deposited HMDSO is considered a suitable material for use in biochip manufacturing.[28] Acrylic acids (AACs) not only impart hydrophilicity to surfaces but also facilitate surface functionalization, which is advantageous for sensing and diagnostic purposes. For example, deoxyribonucleic acid (DNA) can be covalently conjugated to carboxylic acid groups present in AAC-based films, which in turn facilitates the detection of RNA/DNA fragments and antibodies.[29]

The present study describes the development of a new methodology for fabricating an open-surface microfluidic device via APPJ-assisted deposition. Hydrophilic AAC tracks were deposited atop an HMDSO layer and subsequently cross-linked to form a bilayer structure. This proposed technique explores the concept of leveraging wettability-patterned surfaces to facilitate directional liquid transport along designated hydrophilic channels (Figure 1).

DOI: 10.1021/acsomega.9b01317
ACS Omega 2019, 4, 16292−16299

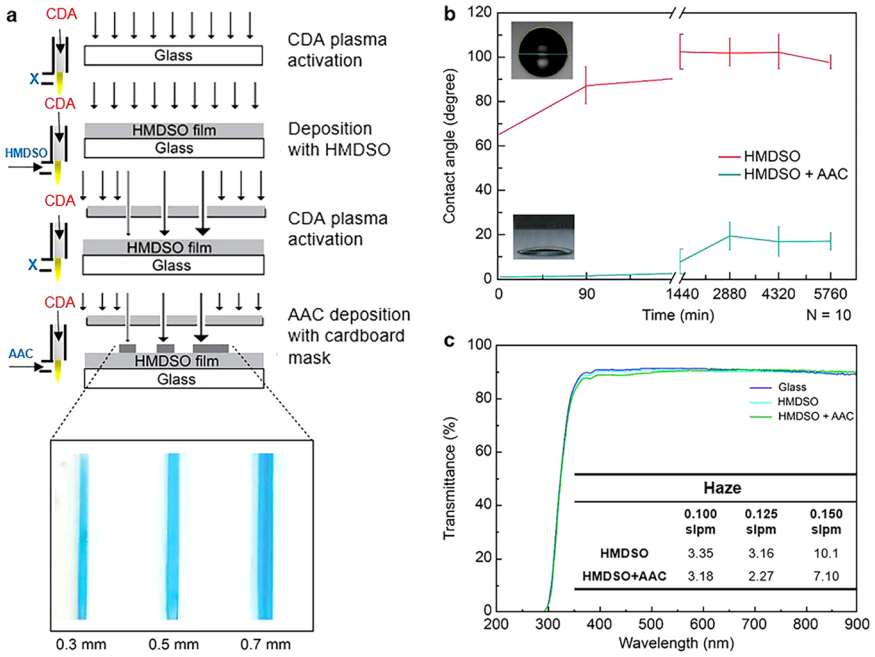

Figure 2. (a) Schematic of the deposition process. The left side of (a) shows the plasma jet settings for different precursors; (b) changes in the contact angles of the HMDSO and AAC films under different exposure times in air; and (c) transmission spectrum response of the HMDSO and AAC thin-film coatings. The table in (c) lists the film haze (%) as a function of the carrier gas flow rate. Haze is the percentage of the incident light exceeding 2.5° to that of the total transmitted light.

Table 1. Parameters of Plasma Treatment

	power (W)	frequency (kHz)	gap (mm)	carrier gas flow rates (slpm)	main gas flow rates (slpm)	temperature (°C)	scan speed (mm/s)
CDA	400	35	15		40		125
HMDSO	400	35	15	0.125	40	36	25
AAC	350	35	15	0.300	40	60	125

RESULTS AND DISCUSSION

Characterization of HMDSO- and AAC-Modified Surfaces. As already described, using the APPJ approach, glass surfaces were hydrophobized herein by depositing a thin HMDSO layer and by exposing sample surfaces to HMDSO plasma for 180 s. The deposited HMDSO layer thickness was estimated as 124 ± 9 nm, as characterized via ellipsometry conducted using the HMDSO-coated silicon wafers prepared under identical deposition conditions. The equilibrium contact angles (θ_C) were measured using the sessile drop method with water as the probing liquid. As observed, the HMDSO-coated glass surfaces exhibited an average θ_C value of 90.5 ± 5.8°, approximately 1.5 h after coating. As indicated by the value of θ_C measuring less than 5°, the corresponding glass surfaces became extremely hydrophilic upon elapse of 4 min after the AAC plasma treatment of the HMDSO-modified glass samples (Figure 2a,b).

Three situations (i.e., surface contamination, free-radical surface energy transfer, and surface energy transfer of the material itself to the rough layer or substrate) could possibly arise, consequently causing the surface energy to drop and the corresponding contact angle to increase.[30] Plasma treatment parameters that could obtain the highest contact angle when forming a HMDSO film are adopted. Table 1 lists the experimental parameters in detail. Figure 2b depicts the changes induced in the contact angle of the HMDSO and AAC films under conditions of different exposure times in air. The experimental results demonstrated that both HMDSO- and AAC-film surfaces effectively maintained their hydrophobic or hydrophilic ability for up to 96 h. The hydrophobic functional groups are deposited on the surface by a dissociation plasma reaction, and the surface is dominated by the formation of a hydrophobic functional CH_3 group. In this study, clean dried air (CDA) is used as the main gas, and oxygen in the CDA participates in the reaction. There are partial hydrophilic groups or long half-life free radicals deposited into the hydrophobic structure. After a certain amount of time, once the hydrophilic groups and the free radicals react with the air to lose their activity (surface passivation), the characteristics of the hydrophobic functional groups are fully expressed; thus, the contact angle increases. Therefore, when the surface passivates and hydrophobic recovery occurs, the hydrophobic properties rapidly manifest. The rise of the contact angle is approximately 40°. Compared with the hydrophobic part, no other hydrophobic functional group reacts with the deposition process, after the hydrophilic surface is passivated; solely, the airborne contaminants lead to the hydrophobic recovery. The hydrophilic group, after the HMDSO coating is completed, is fixed on it by AAC to increase the hydrophilic group of the surface. When the hydrophilic group is corroborated to be fixed on the surface, the hydrophilicity will soon be determined. The contact angle is observed to be >10°. Similarly, during this process, some active plasma reactants or nonbonded molecules remain on the surface; thus, the contact angle will increase when hydrophobic recovery occurs. However, the AAC molecules that have been immobilized

DOI: 10.1021/acsomega.9b01317
ACS Omega 2019, 4, 16292−16299

on the surface exert a hydrophilic effect; therefore, there is a smaller increase in the contact angle (approximately 15−20°).

On tilting the glass substrate by 30°, the droplet flowed along the HMDSO- and AAC-modified glass without diffusion. We first drop 5 μL water droplets on the tilting substrate and then measured the contact angle of the droplet on the track surface, a HMDSO-modified hydrophobic film with an AAC-modified hydrophilic film on glass. The receding angle (uphill) and advancing angle (downhill) are measured as 28.5 ± 5.5 and 22.5 ± 3.5°, respectively, as shown in Figure S1.

The optical transparency of the modified glass was evaluated by measuring the transmittance in the wavelength range of 300−900 nm via an enzyme-linked immunosorbent assay (ELISA) reader (Figure 2c). The plasma-polymerized HMDSO- and AAC-modified glasses exhibited a nearly constant transmittance when compared with that of the unmodified glass. This result suggests that plasma-induced deposition is a versatile technique for depositing a thin layer of optically transparent HMDSO coating. The best parameter combination determined herein corresponded to 400 W of plasma power, 0.125 standard liters per minute (slpm) flow rate of the carrier gas, and 15 mm of nozzle-to-glass distance. Using the above-mentioned combination of parameter values, the deposited SiOx film demonstrated light transmittance exceeding 90% with a corresponding water droplet contact angle of 90°, which ensured the manifestation of the hydrophobicity of the coated glass. Accordingly, the haze of films was measured using a haze machine (Figure 2c). The film haze tended to influence the scattering rate. A film-coating penetration exceeding 90% and a contact angle greater than 90° were considered as the optimum parameters herein. In addition, the experimental design revealed that the carrier gas flow rate significantly affected the contact angle. For instance, the contact angle was observed to have reduced to 85° (below expectations) when the flow rate decreased to 0.100 slpm. The corresponding film haze significantly increased (10.1% at 0.150 slpm in comparison with 3.16% at 0.125 slpm) when the flow rate increased to 0.150 slpm, although the contact angle only increased to 92°. Thus, a carrier gas flow rate of 0.125 slpm for HMDSO was considered optimum. Furthermore, the carrier flow rates had no influence on the transparency and haze for AAC. These results indicate that surface modification with AAC plasma can indeed impart surface hydrophilicity, which is important for creating patterns suitable for inducing surface-tension-driven flow, while optical transparency ensures that the device remains suitable for use in optical characterization techniques.

The surface characterization of the samples at each process stage was conducted via X-ray photoelectron spectroscopy (XPS) (VG Scientific Microlab 350) using Al Kα1,2 (1486.6 eV) excitation. The corresponding energy resolution was approximately 0.1 eV. Figure 3 depicts the X-ray photoelectron spectroscopy (XPS) results obtained for surface elements comprising twin-layered films of HMDSO−glass and AAC−HMDSO−glass. The survey-scan spectra were constructed at a pass energy of 20 eV, while individual spectra for C 1s, Si 2p, and O 1s were fixed at a pass energy of 20 eV with a 0.1 eV energy step. Figure 3 shows that the chemical bonds mainly consisted of C−H and C−C functional groups. Furthermore, the surface still contained a few exposed CH_3 groups; hence, the contact angle of this specimen reached 90° in the contact angle measurements. Clean dried air (CDA) plasma was used to oxidize and remove all CH_3 groups on the HMDSO surface

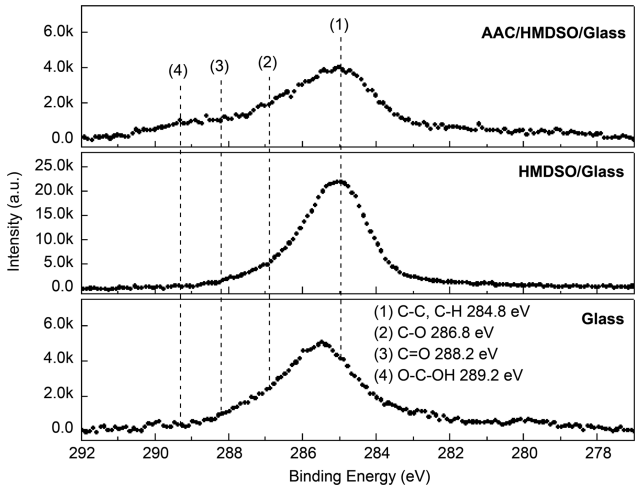

Figure 3. XPS measurements of the deposition process.

prior to the gaseous coating of AAC to ensure that AAC successfully binds to HMDSO. In Table 2, most contaminants

Table 2. Elemental Compositions of the Modified Surface

precursor	Si 2p (atom %)	C 1s (atom %)	O 1s (atom %)
glass (CDA)	26.19	3.01	70.8
HMDSO/glass (CDA)	28.72	10.4	60.87
CDA/HMDSO/glass (CDA)	28.04	3.15	68.81
AAC/CDA/HMDSO/glass (CDA)	31.01	2.71	66.28

on the glass surface were eliminated via plasma treatment (C 1s atom <3%). However, the oxygen content of the surface was greater than Si/O = 1:2 (the Si/O ratio of the pure glass SiO_2 structures) because of the oxidizing effects of plasma. When HMDSO is plated, as the main structure of HMDSO is $O[Si(CH_3)_3]_2$, the content of C 1s increases to 10.4%. In the following process, CH_3 reacts with oxygen in CDA to form a gaseous molecule of H_2O and CO_2 escapes, so it drops to 3.15%, and the oxidized component increases, so the oxygen is increased to 68.81%. When preparing AAC, the main gas used is also CDA; thus, plating AAC may also cause the CH_3 group of the surface to come off the surface again. Therefore, when preparing AAC, the selected plasma wattage is close to the lowest excitation wattage of the machine, which is 350 W (as summarized in Table 1). The contact angle reduced to 16° after AAC coating because of the presence of COOH polar groups on the surface. In addition, the carbon content of the surface was quite low because AAC reacted with CDA (working gas) to form gases like CO_2 during the atmospheric plasma spraying process. Moreover, only a fraction of the AAC molecules was retained by the surface. The AAC introduced in the XPS chart shows the presence of COOH functional groups, but overall the proportion of carbon is reduced (2.71%) and the oxidized portion is also reduced (66.28%), indicating that some of the original surface of CH_3 or AAC fragments still form a gaseous detachment surface; thus, the Si ratio increases slightly. Table 2 summarizes the elemental compositions of the samples.

Design Configuration. The aluminum plate is a rigid and good material to serve as a mask for hydrophobic/hydrophilic patterning (Figure 4a). However, an aluminum-based mask is

DOI: 10.1021/acsomega.9b01317
ACS Omega 2019, 4, 16292−16299

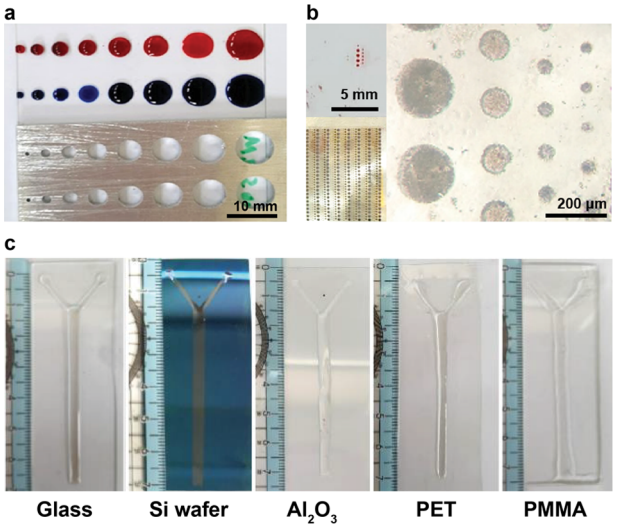

Figure 4. Design of masks and patterns on different substrates: (a) aluminum mask, (b) shadow mask, and (c) patterns on different substrates (i.e., glass, silicon wafer, aluminum, plastic (PET), and acrylic (PMMA) plates).

relatively expensive and requires a precise computer numerical control milling process to create desirable patterns. Interestingly, high-resolution patterns (i.e., 30−200 μm wide) using a shadow metal mask and plasma coating are achieved in Figure 4b. Figure 4b shows optical microscopic images of the patterned film created using a shadow mask. The disadvantages of this method include high cost and a complicated process for mask fabrication. Therefore, a rapid and low-cost mask preparation approach is required. We employed herein a laser cutter to prepare a patterned cardboard to be used as a mask for generating hydrophilic channels. Using a cardboard is beneficial because it is inexpensive. The usage of the laser cutter facilitates rapid prototyping in an economical manner. A minimum line width of 0.3 mm can be achieved herein, and this was within the achievable value limited by the operational range of the laser cutter (Figure 2a). The same approach can be used to pattern various substrates, including glass, silicon wafer, aluminum, plastic (polyethylene terephthalate (PET)), and acrylic (poly(methyl methacrylate) (PMMA)) plates (Figure 4c).

Microfluidic channels were manufactured using atmospheric-plasma-assisted coatings by employing simple cardboard masks. Unlike the conventional photolithography fabrication of a closed microfluidic device, open microfluidic device fabrication avoids the need for chip bonding. An atmospheric-plasma-assisted patterning method was used to simplify the fabrication process, and a virtual wall, instead of a physical microchannel, was constructed. The mask configurations designed for common microfluidic channels in a closed microfluidic device are discussed below. Four different configurations were designed in this study. A prototype of the mask to be used in various microfluidic applications was fabricated in accordance with the design depicted in Figure S2. The said mask was used to fabricate patterns such as straight, mixing, and splitting, with no branching points. In devices comprising grading channels, such as concentration gradient generators (CGGs), many merged channels flow orthogonally. We fabricated the mask featuring two parts, comprising a network of vertical and horizontal channels. Thus, two different mask layers were required to be fabricated and precisely aligned. The first mask layer was attached by aligning it to the rear side of the glass. Figure 5a depicts the design of

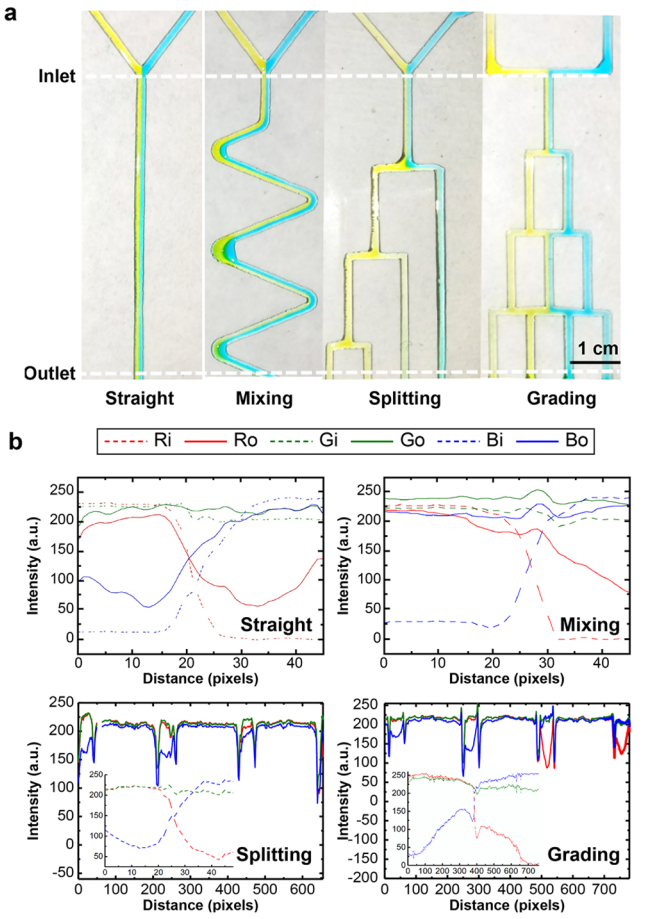

Figure 5. (a) Flow along different patterns (i.e., straight, mixing, splitting, and merging channels) (450 pixels = 1 cm) and (b) red−green−blue (RGB) analysis of the flow. Moreover, the inserted graphs inside the splitting graph and grading graph are the inlet flow distributions of the RGB analysis.

the first layer mask demonstrating a CGG pattern with branched cuts. The second mask layer presented a geometry identical to the CGG pattern, albeit sans branched cuts. The upper limit of the number of masks to be used is two for all microfluidic pattern geometry applications.

Liquid Transport and Mixing on the Proposed Platform. The device was tilted, and gravity was used for driving the fluid flow. The experiment was conducted by setting the tilt angle to 30° in all of the experiments except when observing different flow rates in grading channels that are tilted by 70° (Figure S3). The force of gravity on the liquid was observed to be greater when the inclination angle and/or volume flow rate were increased. The experiment was conducted by setting the tilt angle of grading channels to 70° to observe the influence on grading.

The possibility of a laminar flow through hydrophilic channels of diverse shapes at low volume flow rates is discussed in the paragraphs that follow (Figure 5a).The color composition included red, green, and blue. During the RGB analysis of the image, the inlet RGB was set as R_i, G_i, and B_i, while the outlet RGB was set as R_o, G_o, and B_o. Figure 5b depicts the analysis of liquid transport and mixing on the

DOI: 10.1021/acsomega.9b01317
ACS Omega 2019, 4, 16292−16299

platform. If the value of R/B exceeded 1, more of the yellow color could be observed within channels. Meanwhile, R/B measured less than one. More of the blue color was correspondingly observed. A laminar flow was maintained at the Y-junction (straight line). A single color was observed for the Y-junctions (straight channels) depicted in Figure 5a,b. In the serpentine-shaped microfluidic channels, the R/B color ratio on the left inlet was observed to exceed unity, while that on the right inlet measured less than one. No single color distribution was observed at the outlet of the mixing channels. The observed RGB distribution changed from being symmetric at the inlet to radial at the outlet, thereby denoting that the colors tended to mix.

Regarding the splitting-pattern channels, a single color was observed at the Y-junction in the straight channel within which a laminar flow was maintained. For the inlets at the Y-junctions, the R/B color ratio at the left inlet exceeded one, whereas that at the right inlet measured less than unity. As observed, the color distribution maintained a single color at the outlet. At the splitting channel, four peaks were observed in the RGB distribution. The R/B ratio at each channel was 1.09:2.02:1.05:0.95, thereby indicating that liquid color on the three left outlets demonstrated a more yellow tint, whereas that on the right outlet demonstrated a more bluish tint.

In the two-inlet−four-outlet grading channel network, the two streams injected into the inlets were mixed with neighboring streams in different manners as they flowed through the grading channel network on the open surface. A laminar flow was observed in the straight line when the left (yellow colored) and right (blue-colored) streams flowed from their respective inlets toward the Y-junction (inlet to the B = 1 layer). The two-colored streams were observed to flow toward the left and right sides at the first branch point. Thereafter, the said streams were divided into splitting channels (V = 0, 3). The R/B ratio in the V = 3 channel was equal to 1.24, whereas that in the V = 0 channel was equal to 0.84. After splitting, the two streams recombined in the merging channel on the B = 2 layer. The R/B ratio was equal to 0.45 in the V = 1 channel and 1.62 in the V = 2 channel. In a system of grading channels, the RGB distribution of the color produced in each of the split channels was observed to correspond to the situation wherein liquid flow was directed within the constraints of a patterned virtual hydrophobic wall. Figure S3 indicates that even with the tilt angle being increased to 70° the grading channels maintained their microfluidic function with the liquid flow rate varying in the range of 1−40 mL/min, as shown in Figure S3 (see the Supporting Information (SI)). The results showed that each device had an ability function (Y for separating, S for mixing and splitting, and CGG for different color distribution gradients produced). The proposed open-surface microfluidic platform fabricated using APPJ exhibits great potential for use in disease diagnosis applications. In the case of a hydrophobic film, due to film deposition under atmospheric pressure, the HMDSO film does not exhibit oleophobic characteristics.[21] The hydrophobic angle of the *n*-hexadecane on the HMDSO-modified film is 26°, owing to which the device is more suitable for water-based solutions. Both the AAC film and the HMDSO film are oleophilic. In the oil wettability sample, an oleophobic substrate such as tempered glass can be served as the substrate applied for the oil wettability system. Under a tilt angle of 30°, the yellow oil dye (paraffin oil) and the blue water liquid are mixed at the Y-junction and oil droplets generated in the channel by the shear force, as shown in Figure S4 (SI).

A qualitative mixing (diffusion) test was conducted as shown in Figure S5 (SI). The hydrophilic track was divided to separate reactant area and then coated with a protein assay dye and bovine serum albumin (BSA), respectively. On tilting the substrate at 30°, we observed that the device allowed different regions of the liquid to react and the mixing and reaction times could be controlled by the length of gaps. The liquid front came through a gap of 2 mm in nearly 1.5 s. We observed the mixing (diffusion) reaction; the color turned from red to blue as the liquid diffused from the protein region to the dye region but did not spread. Finally, the device can be reused by washing with deionized water.

CONCLUSIONS

This study reported the development and use of a simple, low-cost, and economical method for fabricating open-surface microfluidic platforms. The proposed design strategy is surface-material-independent and can be equally applied to sapphire, PET, PMMA, and silicon wafers. The APPJ treatment represents an alternate method designed to meet the ever-increasing need to develop a low-cost, easy-to-manufacture microfluidic prototype. Four different device types were fabricated herein. The experimental results obtained demonstrated differences in the wettability of the patterned films and the possibility for laminar flow on these four types. The contact angle measured more than 90.5 ± 5.8° for the hydrophobic film and less than 16° for the hydrophilic films for the same aging time. In conclusion, the proposed method of fabricating patterned films for microfluidic channels possesses the ability of confining liquid to flow along the designated pathways. This methodology may be equally applied to other substrates, oil-based solutions, and qualitative mixing considered to be of potential interest in microfluidic applications.

EXPERIMENTAL SECTION

Materials. HMDSO and AAC were purchased from Alfa Aesar and used as received (condition purity >98%). Food color dye tartrazine (Food Drugs and Cosmetic Yellow No. 4), yellow oil dye (paraffin oil), and Brilliant Blue FCF (Food Drugs and Cosmetic Blue No. 1) were purchased from First Chemical Co., Ltd. (Taiwan). BSA was purchased from Promega Madison, WI. The protein assay dye reagent concentrate was purchased from Bio-Rad (cat. #50000006).

Fabrication of the Open-Surface Microfluidic Platform. A glass slide was used as a substrate for fabricating the proposed open-surface microfluidic platform. The slide measuring 7.6 × 2.6 × 0.1 cm^3 was cleaned with isopropyl alcohol and CDA plasma. A cardboard mask (7.6 × 2.6 × 0.1 cm^3) was fabricated using a laser-cutting machine (Taiwan 3 Axle Technology Co., Ltd./DC5030B). The coatings were deposited using an APPJ system (Figure 1). The coating procedure was conducted using an atmospheric plasma jet with a mixture of the main gas (CDA) and precursors. CDA was used as the working gas to generate plasma in all experiments, and the flow rate of the main gas CDA was 40 slpm. HMDSO and AAC were used as precursors (Figure 2a). The surface was first activated by CDA plasma and then hydrophobized using HMDSO by injecting it into the plasma generating chamber at the end of the nozzle using Ar as the carrier gas on a water bath (temperature, 36 °C). The scanning times are 10 and 1 for

DOI: 10.1021/acsomega.9b01317
ACS Omega 2019, 4, 16292−16299

CDA activation and HMDSO deposition, respectively. The carrier gas flow rates were controlled using a mass-flow controller (ALICAT MC Series). The flow rate of carrier gas was set as 0.125 slpm for HMDSO. A patterned cardboard mask dimension of 7.6 × 2.6 × 0.1 cm^3 was subsequently clamped onto the HMDSO-modified glass. Prior to the coating of the AAC film, CDA plasma was used to activate the surface that was clamped by the mask. Track-patterned hydrophilic layers were deposited on the hydrophobic HMDSO film using AAC as a precursor with a carrier gas flow rate of 0.3 slpm on a water bath temperature of 60 °C. The sweep times of scan injection for the AAC layer as well as the CDA plasma depend on the shaped patterns. The working distance between the jet and the sample was set as 15 mm. AC power was used as the plasma power supply in all experiments, with a 1−600 W output power range; the frequency was fixed at 35 kHz. Table 1 summarizes the experimental parameters used during the fabrication of the proposed open-surface microfluidic devices. The mean total time of fabrication is 16 min; out of this, it takes 1 min to cut a mask, 1 min to prepare the plasma jet equipment, 1 min to expose the sample surfaces to CDA plasma, and 3 and 10 min to deposit the HMDSO and AAC layers, respectively (the scan time for the AAC layer depends on the pattern shaped; the average time is 10 min).

Characterization of the APPJ Films. All film thicknesses were measured via ellipsometry (Mission Peak Optics, Inc., MP100-ST). The water contact angles in air were measured using the sessile drop method employing a contact angle system (First Ten Angstroms 125) with a drop size of 5 μL and a contact angle (θ_C) measured at least 10 times to obtain the mean value and the corresponding standard deviation. Transmittance measurements were conducted using an ELISA reader (Thermo Scientific, Multiskan TM, Go). The haze of films was measured using a haze machine (Gardner BYK). The surface functional groups of the modified films were measured via X-ray photoelectron spectroscopy (VG Scientific Microlab 350). The film was exposure to atmospheric oxygen, between the sample preparation and insertion into XPS chamber, for a maximum of 0.5 h.

Liquid Transport and Mixing Test. Aqueous solutions were dyed using food color. Streams of yellow- and blue-colored water at their respective inlets were mixed together in channels of 1 mm width using syringe pumps at a volume flow rate of 10 μL/min and driven by gravity from the tilt platform at 30°. The two streams were made to enter from the top inlets at the same flow rate and mixed as they flowed downstream. Oil solutions were dyed using oil dye and flow at the above-mentioned parameters. We set up a cell phone parallel to the tilt plate to take photographs. The color information was obtained by an image-analysis software (ImageJ, ver. 1.52a). For a qualitative mixing (diffusion) test, we coated a track with a 1 μL of 5× diluted protein assay dye and 20 μg of bovine serum albumin (BSA) at temperatures of 80 and 37 °C for 30 and 10 min, respectively. Deionized water (5 μL) was flown from the BSA-coated region to the protein assay dye-coated region when the platform was slid at a tilt angle of 30°.

■ ASSOCIATED CONTENT

Supporting Information

The Supporting Information is available free of charge on the ACS Publications website at DOI: 10.1021/acsomega.9b01317.

Sliding of 5 μL of water droplets against the HMDSO- and AAC-modified wettability-patterned surface tilted at 30°; design of first and second masks; grading channels with different flow rates for a tilt angle of 70°; oil wettability test using a Y-junction channel for a tilt angle of 30°; and mixing test (diffusion) using separate regions coated with BSA and protein assay dye for a tilt angle of 30° (PDF)

■ AUTHOR INFORMATION

Corresponding Authors

*E-mail: liborran@g2.nctu.edu.tw (B.-R.L.).
*E-mail: cshsu@mail.nctu.edu.tw (C.-S.H.).

ORCID

Chen-Yu Huang: 0000-0002-9932-5651
Chia-Chih Chang: 0000-0001-5284-6161
Bor-Ran Li: 0000-0003-2266-680X
Chain-Shu Hsu: 0000-0002-8312-2921

Author Contributions

S.-T.W., C.-Y.H., and B.-R.L. designed the work. S.-T.W. executed the experimental work with help from C.-Y.H. and C.-C.W. S.-T.W. wrote the manuscript in discussion with C.-C.C. and B.-R.L. C.-S.H. guided the project and funding.

Notes

The authors declare no competing financial interest.

■ ACKNOWLEDGMENTS

This study was financially supported by the Ministry of Science and Technology (MOST) of Taiwan (106-2113-M-009-013-MY2, 106-2221-E-009-129-MY3) and the Center for Emergent Functional Matter Science of National Chiao Tung University Featured Areas Research Center Program within the framework of the Higher Education Sprout Project of the Ministry of Education (MOE) in Taiwan.

■ REFERENCES

(1) Hoa, X. D.; Kirk, A. G.; Tabrizian, M. Towards integrated and sensitive surface plasmon resonance biosensors: A review of recent progress. *Biosens. Bioelectron.* **2007**, *23*, 151−160.

(2) Li, B. R.; Hsieh, Y. J.; Chen, Y. X.; Chung, Y. T.; Pan, C. Y.; Chen, Y. T. An ultrasensitive nanowire-transistor biosensor for detecting dopamine release from living PC12 cells under hypoxic stimulation. *J. Am. Chem. Soc.* **2013**, *135*, 16034−16037.

(3) Li, B. R.; Shen, M. Y.; Yu, H. H.; Li, Y. K. Rapid construction of an effective antifouling layer on a Au surface via electrodeposition. *Chem. Commun.* **2014**, *50*, 6793−6796.

(4) Shen, M. Y.; Li, B. R.; Li, Y. K. Silicon nanowire field-effect-transistor based biosensors: From sensitive to ultra-sensitive. *Biosens. Bioelectron.* **2014**, *60*, 101−111.

(5) Chiu, P. L.; Chang, C. H.; Lin, Y. L.; Tsou, P. H.; Li, B. R. Rapid and safe isolation of human peripheral blood B and T lymphocytes through spiral microfluidic channels. *Sci. Rep.* **2019**, *9*, No. 8145.

(6) Yang, C. H.; Hsieh, Y. L.; Tsou, P. H.; Li, B. R. Thermopneumatic suction integrated microfluidic blood analysis system. *PLoS One* **2019**, *14*, No. e0208676.

(7) Mohamed, E.; Schutzius, T. M.; Megaridis, C. M. Inkjet patterned superhydrophobic paper for open-air surface microfluidic devices. *Lab Chip* **2014**, *14*, 1168−1175.

(8) Majhy, B.; Iqbal, R.; Gaikwad, R.; Sen, A. K. Dynamics of capillary flow in an open superoleophilic microchannel and its application to sensing of oil. *Microfluid. Nanofluid.* **2018**, *22*, No. 116.

(9) Thuo, M. M.; Martinez, R. V.; Lan, W.-J.; Liu, X.; Barber, J.; Atkinson, J.; Bandarage, D.; Bloch, J.-F.; Whitesides, G. M. Fabrication of low-cost paper-based microfluidic devices by

DOI: 10.1021/acsomega.9b01317
ACS Omega 2019, 4, 16292−16299

embossing or cut-and-stack methods. *Chem. Mater.* **2014**, *26*, 4230−4237.
(10) Krüger, J.; Singh, K.; O'Neill, A.; Jackson, C.; Morrison, A.; O'Brien, P. Development of a microfluidic device for fluorescence activated cell sorting. *J. Micromech. Microeng.* **2002**, *12*, 486−494.
(11) Morrissette, J. M.; Mahapatra, P. S.; Ghosh, A.; Ganguly, R.; Megaridis, C. M. Rapid, self-driven liquid mixing on open-surface microfluidic platforms. *Sci. Rep.* **2017**, *7*, No. 1800.
(12) Li, C.; Boban, M.; Snyder, S. A.; Kobaku, S. P.; Kwon, G.; Mehta, G.; Tuteja, A. Paper-based surfaces with extreme wettabilities for novel, open-channel microfluidic devices. *Adv. Funct. Mater.* **2016**, *26*, 6121−6131.
(13) Kobaku, S. P.; Kwon, G.; Kota, A. K.; Karunakaran, R. G.; Wong, P.; Lee, D. H.; Tuteja, A. Wettability engendered template self-assembly (WETS) for fabricating multiphasic particles. *ACS Appl. Mater. Interfaces* **2015**, *7*, 4075−4080.
(14) Songok, J.; Toivakka, M. Controlling capillary-driven surface flow on a paper-based microfluidic channel. *Microfluid. Nanofluid.* **2016**, *20*, No. 63.
(15) Ghosh, A.; Ganguly, R.; Schutzius, T. M.; Megaridis, C. M. Wettability patterning for high-rate, pumpless fluid transport on open, non-planar microfluidic platforms. *Lab Chip* **2014**, *14*, 1538−1550.
(16) Melin, J.; van der Wijngaart, W.; Stemme, G. Behaviour and design considerations for continuous flow closed-open-closed liquid microchannels. *Lab Chip* **2005**, *5*, 682−686.
(17) Berthier, J.; Brakke, K. A.; Gosselin, D.; Bourdat, A.-G.; Nonglaton, G.; Villard, N.; Laffite, G.; Boizot, F.; Costa, G.; Delapierre, G. Suspended microflows between vertical parallel walls. *Microfluid. Nanofluid.* **2015**, *18*, 919−929.
(18) Lin, R.; Burns, M. A. Surface-modified polyolefin microfluidic devices for liquid handling. *J. Micromech. Microeng.* **2005**, *15*, 2156−2162.
(19) Dang, K.; Morrison, D. W.; Demirci, U.; Khademhosseini, A. Plasma in Microchannel. In *Encyclopedia of Microfluidics Nanofluidics*; Li, D., Ed.; Springer: Boston, MA, 2015; pp 2781−2789.
(20) Schutze, A.; Jeong, J. Y.; Babayan, S. E.; Jaeyoung Park, J.; Selwyn, G. S.; Hicks, R. F. The atmospheric-pressure plasma jet: A review and comparison to other plasma sources. *IEEE Trans. Plasma Sci.* **1998**, *26*, 1685−1694.
(21) Wu, S. T.; Weng, C. C.; Li, B. R.; Hsu, C. S. Fabrication of magnetic liquid marbles using superhydrophobic atmospheric pressure plasma jet-formed fluorinated silica nanocomposites. *J. Mater. Sci.* **2019**, *54*, 10179−10190.
(22) Chang, K.-M.; Ho, P. C.; Wu, C.-W.; Wu, C.-J.; Chang, C.-C. Structural and optoelectronic properties of GZO/SiOx bilayer films by atmosphere pressure plasma jet. *ECS Trans.* **2012**, *45*, 221−229.
(23) Chang, K. M.; Huang, S. H.; Wu, C. J.; Lin, W. L.; Chen, W. C.; Chi, C. C.; Lin, J.; Chang, C. Transparent conductive indium-doped zinc oxide films prepared by atmospheric pressure plasma jet. *Thin Solid Films* **2011**, *519*, 5114−5117.
(24) Chang, K. M.; Ho, P. C.; Ariyarit, A.; Yang, K. H.; Hsu, J. M.; Wu, C. J.; Chang, C. C. Enhancement of the light-scattering ability of Ga-doped ZnO thin films using SiOx nano-films prepared by atmospheric pressure plasma deposition system Ga. *Thin Solid Films* **2013**, *548*, 460−464.
(25) Zhao, B.; Moore, J. S.; Beebe, D. J. Surface-directed liquid flow inside microchannels. *Science* **2001**, *291*, 1023−1026.
(26) Oliveira, N. M.; Neto, A. I.; Song, W. L.; Mano, J. F. Two-dimensional open microfluidic devices by tuning the wettability on patterned superhydrophobic polymeric surface. *Appl. Phys. Express* **2010**, *3*, No. 085205.
(27) Bouaidat, S.; Hansen, O.; Bruus, H.; Berendsen, C.; Bau-Madsen, N. K.; Thomsen, P.; Wolff, A.; Jonsmann, J. Surface-directed capillary system; theory, experiments and applications. *Lab Chip* **2005**, *5*, 827−836.
(28) Morent, R.; De Geyter, N.; Van Vlierberghe, S.; Dubruel, P.; Leys, C.; Schacht, E. Organic−inorganic behaviour of HMDSO films plasma-polymerized at atmospheric pressure. *Surf. Coat. Technol.* **2009**, *203*, 1366−1372.
(29) Ricciardi, S.; Castagna, R.; Severino, S. M.; Ferrante, I.; Frascella, F.; Celasco, E.; Mandracci, P.; Vallini, I.; Mantero, G.; Pirri, C. F.; Rivolo, P. Surface functionalization by poly-acrylic acid plasma-polymerized films for microarray DNA diagnostics. *Surf. Coat. Technol.* **2012**, *207*, 389−399.
(30) Vandenbossche, M.; Hegemann, D. Recent approaches to reduce aging phenomena in oxygen- and nitrogen-containing plasma polymer films: An overview. *Curr. Opin. Solid State Mater. Sci.* **2018**, *22*, 26−38.

DOI: 10.1021/acsomega.9b01317
ACS Omega 2019, 4, 16292−16299